Applied Surface Science Advances 19 (2024) 100574

Contents lists available at ScienceDirect

Applied Surface Science Advances

journal homepage: www.sciencedirect.com/journal/applied-surface-science-advances

Tailoring AA6063 for improving antibacterial properties

M. Medel-Plaza [a], A. Conde [b,c], J.J. de Damborenea [b,c], J.J. Aguilera-Correa [a,c], J. Esteban [a,c], M. A. Arenas [b,c,*]

[a] Department of Clinical Microbiology. IIS-Fundación Jiménez Díaz, UAM. Avda. Reyes Católicos, 2. 28040 Madrid, Spain
[b] National Centre for Metallurgical Research, CENIM-CSIC, Avda. Gregorio del Amo, 8., Madrid 28040, Spain
[c] CIBERINFEC-CIBER de Enfermedades Infecciosas, Instituto de Salud Carlos III, Madrid 28029, Spain

ARTICLE INFO

Keywords:
Antibacterial properties
Aluminium alloys
Anodizing and cerium

ABSTRACT

Aluminium alloy 6063 was subjected to two different surface treatments: anodizing in sulphuric acid (SA) and the deposition of cerium conversion coatings (CeCC), in order to evaluate the antibacterial properties of the new surfaces. The microstructure and composition of the anodized samples and the cerium conversion coatings were characterized by scanning electron microscopy, energy dispersive spectrometry (SEM/EDS) and X-ray Photoemission Spectroscopy (XPS). Roughness and wettability were measured for all new surfaces. Bacterial adherence studies were carried out using *Pseudomonas aeruginosa*, with promising results for the anodized samples.

1. Introduction

In the last decade, the extremely important role of metallic surfaces in the transmission of infectious agents has been highlighted. The influenza A(H1N1) pandemic of 2009–2010, revealed the lack of information on viral survival on different household surfaces. Greatorex *et al.* [1] demonstrated that influenza A strains could survive up to nine hours on a wide variety of metallic surfaces. During the COVID-19 pandemic, the role of metallic surfaces was again put on the table. Although for SARS-CoV2 the airborne transmission is the main route for virus spread and rapid contagion, this is not the case for other viruses and bacteria where contaminated surfaces can be used as indirect transmission of infection. The mechanism of surface infection transmission through surfaces is simple: the droplets from sneezing or coughing are deposited on fomites and spread when a person comes into contact with the contaminated surface through their hands [2].

Stephens and co-workers [3] reviewed the contamination by microbial communities and antibiotic-resistant bacteria in different fomites. Gram-positive and negative bacteria can survive for months on inanimate surfaces and are a risk factor for nosocomial infections [4]. Of particular note mention are *Staphylococcus aureus* and *Pseudomonas aeruginosa*, currently the most commonly co-infecting bacteria in severe nosocomial infections, apart from other environmental bacteria [5,6].

On the other hand, metallic surfaces are increasingly present in our living environment. Behind steel, aluminium alloys are the most widely used metal in the world due to their excellent properties, i.e. good electrical conductivity, good corrosion resistance and extrudability, relatively low cost and a high-quality surface finish [7]. For these reasons, aluminium alloys are widely used in transport, hydraulic systems, mining equipment, nuclear technology and construction industries among others. Of particular importance, however, are everyday items such as door frames, handrails, furniture, appliances and kitchenware, which are touched by thousands of people every day. Much of this equipment (lifts, stairs, benches, kitchen appliances, handrails, handles or trays) is made from AA6063 aluminium alloy.

As mentioned above, in recent years a particular emphasis has been placed on providing these alloys not only with new functionalities to extend their service life, but also with antimicrobial properties to prevent the pathogenic microorganisms from remaining active on inanimate surfaces for long periods.

Adhesion of microorganisms to a surface is a complex process that depends on several factors such as the type of microorganism (virus or bacteria), even strain variations, the properties of the surface -topography, roughness, chemistry-, the surrounding environment - temperature and relative humidity-, the time of exposure and the inoculation dose [8]. Therefore, although the microbial adherence is controlled by many biological and physicochemical factors, surface properties have been shown a key factor in their adherence and survival on surfaces [9]. Despite the extensive research performed on different substrates, it is still not clear which surfaces characteristics favour adhesion, as they are often interrelated. Nevertheless, the use of antimicrobial surfaces can be a complementary strategy to the disinfection and cleaning practices that

* Corresponding author.
E-mail address: geles@cenim.csic.es (M.A. Arenas).

https://doi.org/10.1016/j.apsadv.2024.100574
Received 2 November 2023; Received in revised form 22 December 2023; Accepted 19 January 2024
Available online 25 January 2024

have been investigated to protect surfaces from contamination. Recently, efforts have been focused on the development of surface treatments to provide advanced functionalities related to infections, following different routes [10–12]

However, in order to protect large areas of metallic surfaces (e.g. handrails or handles), a cheaper and more effective method is required. Anodizing is perhaps one of the most commonly processes used for aluminium alloys in commercial applications due to its simplicity and low cost, making anodized aluminum-based materials very interesting candidates for use on high-touch surfaces [13].

Another way to improve the antimicrobial properties of aluminium alloys is to deposit coatings on their surface that can mitigate the attachment of microbial pathogens. Over the last three decades, cerium conversion coatings have been investigated for the corrosion protection of aluminium alloys as an alternative to chromate-based treatments because they are less toxic and environmentally friendly. In recent years, cerium nanoparticles –NPs- have attracted considerable interest as an antimicrobial agent [14]. The use of CeO_2 in industrial and biomedical applications is due to its ability to reduce Ce^{+4} to Ce^{+3} on the surface of CeO_2 NPs [15,16]. It has been reported that the Ce^{4+} cation of the nanoparticles is reduced to Ce^{3+} at the membrane surface of *Escherichia coli,* resulting in oxidative stress of the main components of the plasma membrane of the microorganism, such as lipids and/or proteins, or during cellular metabolism electron uptake [17]. Another proposed mechanism of antibacterial action is the generation of ROS by metal NPs, which that leads to the induction of oxidative stress and alters the function of the respiratory chain in bacteria [18].

This property widely reported for CeO_2 NP has also recently been reported when cerium is incorporated into coatings. Pedroi et al. [19] studied the antimicrobial activity of Ce–doped hydroxyapatite suspensions (5 Ce–Hap) and Ce-doped hydroxyapatite coatings using gram-positive *S. aureus* ATCC 25,923, gram-negative *E. coli* ATCC 25, 922, and fungal *Candida albicans* ATCC 90,029 at different time points. The results showed that both 5Ce–HAp suspensions and 5Ce–HAp coatings effectively inhibited the development of colony forming units (CFU) for all the microbial strains tested and they attributed the antimicrobial effect to the presence of cerium ions in the lattice of the hydroxyapatite.

The aim of the present work is to modify the surface of the aluminium alloy AA6063 by anodizing and deposition of cerium conversion coatings in order to study the bacterial adherence of an environmental species, *P. aeruginosa,* to the alloy surface. A morphological and compositional characterization of the modified surfaces was carried out as well as bacterial adhesion tests.

2. Materials and methods

2.1. Material and surface treatments

15 mm diameter bars of a commercial aluminium alloy 6063-T5 supplied by ALU-STOCK were used. The test samples were cut into discs 2 mm thick. Table 1 shows the chemical composition of the commercial aluminium alloy 6063-T5 as given in the certificate supplied by the manufacturer.

Depending on whether the samples were anodized or conversion coated, different surface pretreatments were required. For anodization, the samples were ground up to 1200 SiC, rinsed in deionized water and in ethanol. Alkaline etching was then carried out in a 0.6 M NaOH solution at 40 °C for 300 s followed by desmutting for 15 s in a 7.2 M HNO_3 solution at room temperature. Prior to anodizing, the untreated parts of the samples were masked with a special lacquer. The anodizing process was carried out in a two-electrode cell where the cathode was a stainless steel ring. The anodizing process was performed in an aqueous solution of 0.4 M sulphuric acid (H_2SO_4) at 35 °C (SA) applying a stepped voltage of 4 V/min from 0 to 20 V and then at constant voltage of 20 V for 6 min. Anodized samples were rinsed in deionized water for 45 min to remove the residual acid within the nanoporous structure.

The thickness of the anodic layer was measured using a Fisherscope probe.

For the deposition of Cerium Conversion Coatings (CeCC), the samples were also ground up to 1200 SiC and polished with diamond paste to 3 μm using standard metallographic techniques. For the deposition of CeCC, the samples were immersed in a cerium conversion bath containing 10,000 ppm $CeCl_3{\cdot}7\ H_2O$ + 0.3 vol.% H_2O_2 for 1 h at room temperature. After this time the CeC coated samples were rinsed in distilled water, ethanol and dried in hot air. Table 2 summarizes the sample designations according to the surface treatments applied. Seven samples were prepared for each condition.

2.2. Surface characterization

Scanning electron microscopy (SEM) was used for compositional and morphological analysis of the anodic layers (surface and cross sections) and the cerium conversion coatings, using a Hitachi S- 4800 equipped with an energy dispersive X-ray (EDX) instrument. At least five EDS analyses were performed on each type of particle or zone to determine the semiquantitative analysis composition in atomic percent (at.%).

In addition, the chemical composition of the cerium conversion layers was studied by X-ray Photoemission Spectroscopy (XPS). The XPS

Table 2
Sample designation according to anodizing and cerium electrolyte composition.

Sample designation	Pretreatment	Treatment	Cleaning	Surface treatment
REF (AE+*D*)	Grind up to 1200SiC, Alkaline etching in 0.6 M NaOH 40 °C for 10 min and desmutting 15 s in 7.2 M HNO_3 solution at T_{room}			None
REF (P)	Grind up to 1200 SiC and polished to 3μm	–	–	None
SA	Grind up to 1200SiC, Alkaline etching in 0.6 M NaOH 40 °C for 10 min and desmutting 15 s in 7.2 M HNO_3 solution at T_{room}	Aqueous solution of 0.4 M H_2SO_4 solution at 35 °C. Stepped voltage of 4 V per minute from 0 to 20 V and then keeping it for 6 min	Rinse in deionized water for 45 min	Anodizing
CeCC	Grind up to 1200 SiC and polished to 3μm	10,000 ppm $CeCl_3{\cdot}7H_2O$ + 0.3 vol.% H_2O_2 for 1 h at RT	Rinse in distilled water, ethanol and dry in hot air	Conversion coating

Table 1
Chemical composition of the aluminium alloy 6063 (weight%).

	Al	Mn	Si	Cr	Cu	Zn	Fe	Ti	Mg
6063-T5	Bal.	0.03	0.54	0.01	0.01	0.01	0.19	0.01	0.52

analysis was performed using a high vacuum VG-CLAM XPS system with a non-monochromatic magnesium anode (Kα 1253.6 eV, 300 W). Spectra were recorded in the normal configuration. Survey spectra were obtained with a pass energy of 150 eV, while high-resolution spectra of O 1 s, Ce 3 d and Al 2 p were obtained with a pass energy of 20 eV. The XPS spectra were analysed by subtracting a Shirley- type baseline and the peak shapes of the main XPS signals were optimized by using an 80:20 and 90:10 Gaussian function: Lorentzian function. All XPS spectra were calibrated in binding energy (BE) using the hydrocarbon-type carbon groups at 284.8 eV in the C 1 s region.

2.3. Roughness and wettability

The average roughness of the samples, R_a, was measured using an optical imaging profilometer Plμ 2300 (Sensofar) with a 20x EPI magnification objective. Roughness measurement was performed with a cut off of 7 in a total evaluation length 560 μm. Data processing was done under ASME B46.1 standard using a two sections gaussian filter (λ_c= 0.08 mm and λ_s =2.5 mm). Roughness measurements were performed in 5 different zones of the sample, collecting 90 measurements on each sample (n = 90) and the roughness parameters data Ra is presented as the mean value and the standard deviation ($\bar{X}$±SD).

Surface contact angles were measured with distilled water using a Theta Attension optical tensiometer (KSV Instruments) with automatic liquid dispenser and monochromatic cold light source, operated in trigger mode with video frames recorded at 60 ms intervals. The drop size was 3 μL and the drop rate was 20 μL/s with a dispensing rate of 2 μL/s. Contact angles were calculated using the Young –Laplace drop profile fitting method. Each contact angle value is reported as the average of 5 measurements taken at different locations on the sample surface. An average of 40 frames was used to calculate the contact angle for each drop. The contact angle value is given as the mean value and the standard deviation ($\bar{X}$±SD).

2.4. Microbiological characterization

P. *aeruginosa* ATCC 27,853 was used as a model of environmental bacterium [20–22] . The strain was stored at −80 °C until the experiments were performed.

The bacterial adhesion experiments on the AA6063 reference, anodized, and cerium-coated samples were performed according to a modification of the methodology previously described by Aguilera-Correa et al. . [23]. Each sample was washed and vortexed for 15 s at 300 rpm in sterile distilled water (B. Braun, Germany) prior to this experiment. The strain was grown in tryptic soy broth (bioMérieux, Marcy-l'Étoile, France) at 37 °C for 24 h. After culture, the bacteria were harvested at 3500 rpm for 10 min. The supernatant was discarded, and the pellet was washed three times with sterile 0.9% NaCl saline solution (SS) (B. Braun). Bacteria were then suspended and diluted in SS, reaching 10^8 colony-forming units per milliliter of bacterial solution (CFU/ml), and 5 ml of this solution was statically incubated on AA6063 samples in a sterile non-treated six-well plate (Thermo Fisher Scientific, MA, USA) at 22 °C for 90 min [24–26]. After incubation, samples were washed three times with SS to remove non-adhered bacteria, as described in the literature [25]. Metallic samples were then stained using a Live/Dead Bac Light bacterial viability kit (Thermo Fisher Scientific, MA, USA) and rinsed with sterile distilled water [27]. Approximately 10 pictures (40x magnification) were taken for each sample with a DM 2000 fluorescence microscope (Leica Microsystems, Wetzlar, Germany). All were taken under the same microscopy conditions (183.3- to 380 ms exposure time, 5.5 × optical gain, 1.50 saturation level and gamma of 10.00). The percentage of the total surface with adhered bacteria as well as the percentages of dead and live bacteria were calculated and analyzed by using ImageJ software (National Institutes of Health, Bethesda, MD, USA). Experiments were performed in triplicate.

Finally, after 90 min of incubation, the bacterial solution exposed to each material was used to estimate the number of planktonic bacteria (colony-forming units per milliliter, CFU/ml) using the drop plate method [28] on MacConkey agar (bioMérieux, Marcy-l'Étoile, France). The remaining volume was used to evaluate the release of aluminium cations (Al) from the reference surface, the anodized surface and the cerium-coated surface as described previously [23]. After 90 min of incubation, 1.5 ml of the supernatant in contact with each material was set aside to measure the Al concentration in the bacterial solution, and at least 2 ml was filtered through a philtre with a pore size of 0.22 m to estimate the concentration of Al uptake by these planktonic bacteria. Using a Perkin Elmer Analyst 600 from Reference Laboratories (Barcelona, Spain), at least 1 millilitre of water was sampled at different times to determine the Al content by atomic absorption spectroscopy. The detection limit was 5 ng/ml in this experiment.

Statistical analysis was performed using Graph Pad Prism 8 software (GraphPad Software, San Diego, CA, USA), and data were analyzed by the non-parametric unilateral Wilcoxon test with a level of statistical significance of p <0.05. Values are cited and presented as median and interquartile range.

3. Results and discussion

3.1. Morphology and chemical composition

Fig. 1 shows the microstructure of the aluminium alloy 6063. Two types of intermetallics were identified: rounded and elongated brighter particles corresponding to α-AlFeSi intermetallics or α-AlMnFeSi intermetallics since Fe can be substituted by Mn and stabilize the formation of the $Al_{12}(FeMn)_3Si$, Fig. 1a; and polygonal darker particles corresponding to Mg_2Si precipitates, Fig. 1b. These results are in agreement with those described in the literature [29,30].

Figs. 2a and 2b show the surface microstructure after alkaline etching and desmutting, and after mechanical polishing, respectively. Bright particles consisting of AlFeSi or AlFeMnSi intermetallics, and dark particles related to Mg_2Si particles can be clearly observed. Thus, the intermetallics in the aluminium alloy 6063 remain on the surface following both pre-treatment processes and play an active role in the anodizing or cerium deposition.

3.1.1. Anodic layers (SA)

After anodization in sulphuric acid, a nanoporous structure is clearly observed in the top view of the anodic layer, Figs. 3a and 3b. Pore size was measured using ImageJ software, indicating a pore diameter of ~16 nm, in agreement with values reported by other authors for anodic layers grown at 20 V in sulphuric acid for aluminium alloys [31,32].

The cross-section of the anodic film shows an oxide layer of quite uniform thickness, Fig. 4. The average thickness of the layer was 7.10 μm, which is in good agreement to the thickness measured using a Fisherscope probe, ~7.08 μm. EDS analysis of the anodic films shows that the anodic film is mainly composed of aluminium, oxygen, silicon and sulphur, Table 3.

The presence of sulphur in the anodic layer is well known in the literature as acid anions are incorporated into the film during the anodizing process. According to the growth mechanism of ionic migration, the main alloying elements in solid solution in the 6063 alloy (silicon and magnesium) are simultaneously oxidized within the aluminium at the alloy/film interface. The outward migration rates of species (cations) in the anodic alumina are related to the metal-oxygen single bond energies compared to Al-oxygen (Al^{3+}-O^{2-}) single bond, with relative rates decreasing as the metal-oxygen single bond energy increases. Therefore, a larger outward migration rate of Mg^{2+} ions relative to that of Al^{3+} ions in anodic alumina should be expected, considering the respective metal-oxygen single bond energies: Mg-O: 167 KJ/mol vs. Al-O: 281 KJ/mol [33–37]. Therefore, the anodic film is depleted of magnesium as a result of the higher outward mobility of

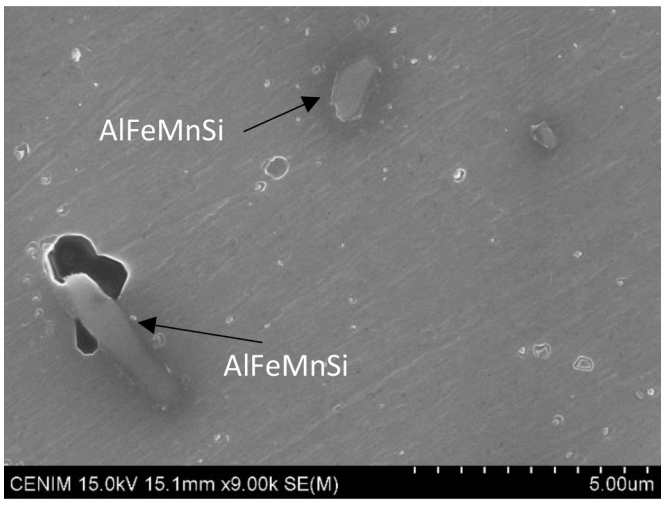

a)

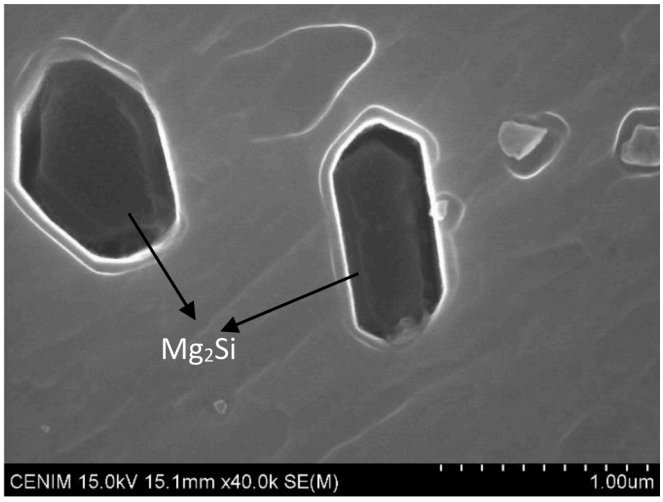

b)

Fig. 1. FEG-SEM micrographs. Microstructure of AA6063 alloy after a metallographic etching with HF for 30 s at room temperature. a) α-AlFeMnSi Intermetallic b) Mg2Si particles.

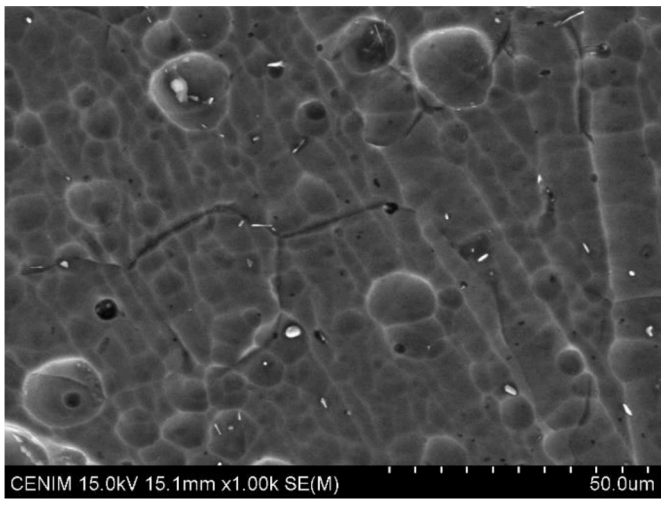

a)

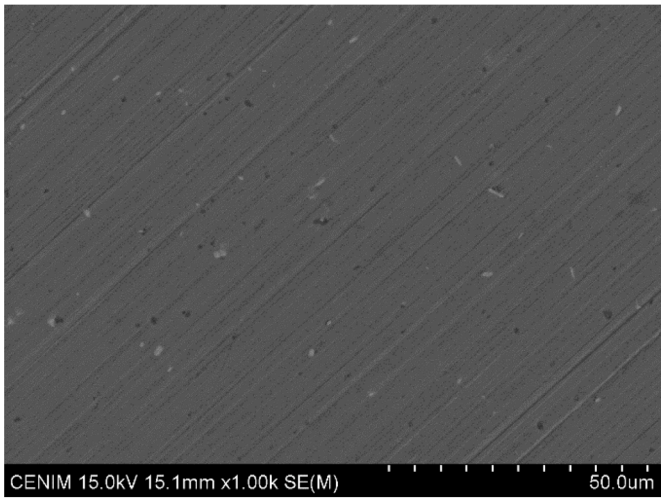

b)

Fig. 2. FEG-SEM micrographs of AA6063 alloy. a) Surface appearance after alkaline etching and desmutting. b) Surface appearance after mechanical polishing.

magnesium species relative to aluminium as confirmed by EDS analysis, see Table 3. Magnesium ions would be lost to the electrolyte on reaching the surface of the film and might be present in the pore together with residual acid. Conversely, as Si-oxygen species have a higher single bond energy than Al-oxygen species: Si-O: 466 KJ/mol vs. Al-O: 281 KJ/mol, silicon species are immobile during the growth of anodic alumina, and are therefore located in the inner film layers [34].

On the other hand, the backscattered electron image of the cross section shows the presence of anodized intermetallic particles trapped in the anodic layer, Fig. 4. The EDS spectra revealed the presence of Al, Fe, Si and Mn in the particles with a bright contrast, corresponding to oxidized alfa- AlMnFeSi, while the particles with a dark contrast have a higher silicon content than the anodic layer and correspond to oxidized Mg_2Si particles. The presence of the oxidized particles in the anodic film results in a significantly reduced rate of oxidation of the silicon particles compared to the aluminium matrix. The more rapid oxidation of the matrix leads to the coarsening of the porous anodic alumina beneath the particle and eventual occlusion of the particle in the anodic film.

3.1.2. Cerium conversion coatings (CeCC)

As previously mentioned, the surface preparation of the samples was different from that used for anodizing. After grinding and polishing, the samples were immersed in the cerium bath for 1 h. When the samples were removed, the color of the surface was slightly yellowish.

SEM analysis revealed the homogenous deposition of a layer with globular features, Fig. 5, and EDS showed the presence of Ce (1.5 at.%), Al (81.82 at.%) and O (16.06 at.%) in the surface, indicating that the cerium conversion coating may be composed of hydroxides and oxides of aluminium and cerium.

Cerium deposition occurs because of the electrochemical difference between aluminium matrix and the main alloy constituents, AlFeSi(Mn) intermetallics, which are cathodic sites respect to the matrix, allowing the deposition in cathodic sites on the surface [38].

The composition of the cerium conversion coating was also analyzed by XPS. Fig. 6a shows the high-resolution spectrum of O1s. As can be seen, the broad peak at binding energy of 531.41 eV can be deconvoluted into three peaks. The first one is placed at 531.6 eV corresponds to

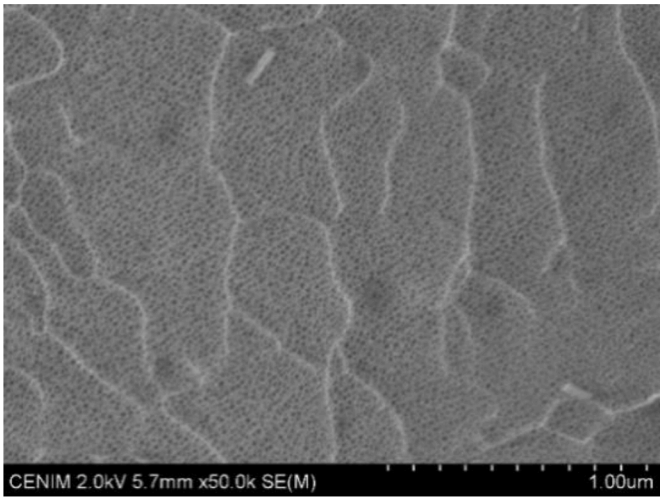

a)

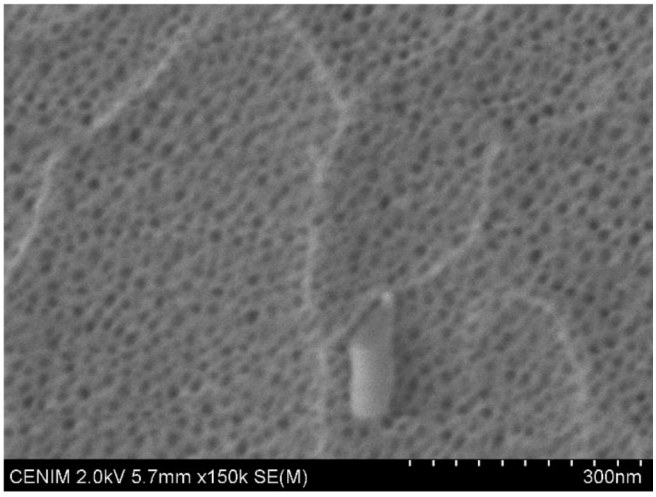

b)

Fig. 3. SEM images. a) Surface morphology of the AA6063 anodized sample surface. b) high magnification micrograph.

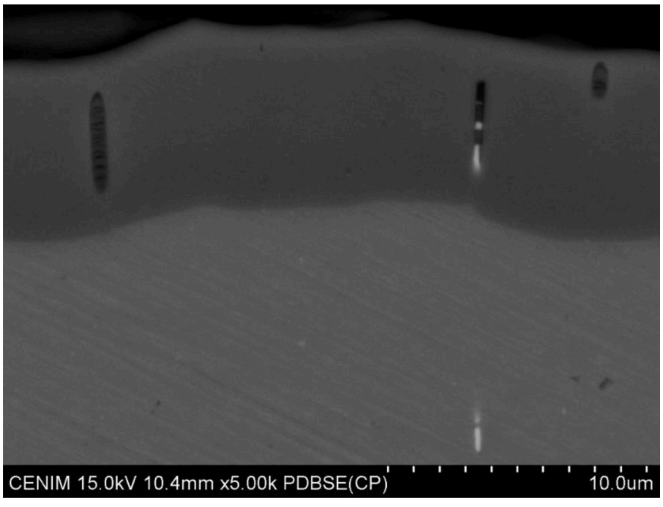

Fig. 4. Cross-section of the anodic film grown in sulphuric acid.

Table 3
Semiquantitative composition of the anodic layer and embedded particles obtained by EDS analysis (in at.%).

	Al	O	Si	Mg	S	Fe	Mn
Anodic layer	33.27	63.68	0.39	–	2.65	–	–
Dark particles in the anodic film	32.87	56.50	7.50	0.09	3.04	–	–
Bright particles in the anodic film	40.22	49.93	3.45	–	1.73	4.44	0.23

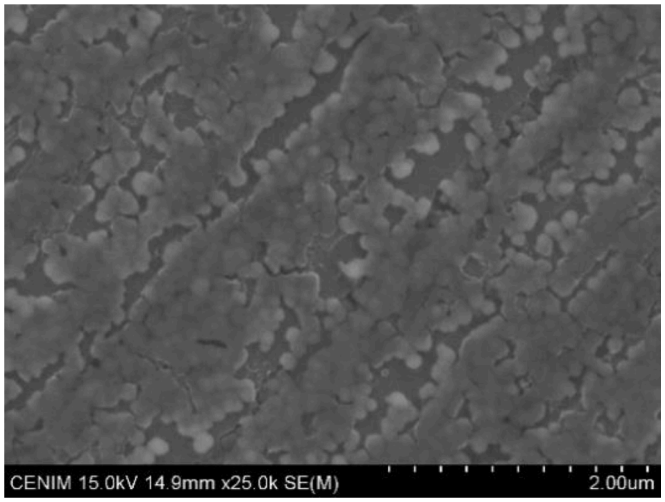

Fig. 5. SEM image. Surface appearance of the cerium conversion coating, CeCC.

alumina and/or aluminium oxihydroxide (AlOOH), the peak at 530.62 eV corresponds to Ce_2O_3 and the last peak at 529 eV corresponds to CeO_2. Fig. 6b depicts the Al 2 p high-resolution spectrum. It is also composed of three components corresponding to: 75.15 eV for alumina, another at 74.73 eV for aluminium hydroxide and finally, a peak related to metallic aluminium at 72.13 eV. Finally, Ce3d high-resolution spectrum, Fig. 6c, shows three peaks. Analyzing from the highest to the lowest binding energy, the first peak placed at 916.25 eV corresponds to the satellite peak u''' of Ce^{4+} which indicates the presence of Ce^{4+} in the coating [39]. In addition, the Ce 3d spectrum is composed of pairs of spin-orbit doublets, indicating the coexistence of Ce $^{3+}$and Ce $^{4+}$. The peaks corresponding to the Ce^{3+} peaks are placed at the following binding energies: 903.64 eV, 885.48 eV and 881.80 eV, whereas those corresponding to Ce $^{4+}$ are at binding energies of 898.45 eV and 900.56 eV. According to the literature, these binding energy values are typical for $Ce^{3+}$and Ce $^{4+}$compounds [40,41].

XPS analysis shows that the cerium conversion coating is mainly composed of a mixture of alumina/aluminium hydroxide and cerium oxides (Ce $^{3+}$ and Ce $^{4+}$).

3.2. Roughness and wettability

Roughness measurements, Ra, are summarized in Table 4. As can be seen, both reference samples -REF (AE+*D*) and REF(P) have lower roughness values than the surface treated aluminium alloys. The anodized samples in shulphuric acid, SA, show the highest roughness in the micrometer range, while the roughness of the CeCC samples is in the nanometer range. Girginov et al. [42] pointed out that the increase in the surface roughness after anodizing is caused by the presence of intermetallics in the anodic film and their gradual dissolution during the process.

Finally, the static water contact angle measurements were carried out on all samples. The reference alloy (AE+*D*) shows a contact angle

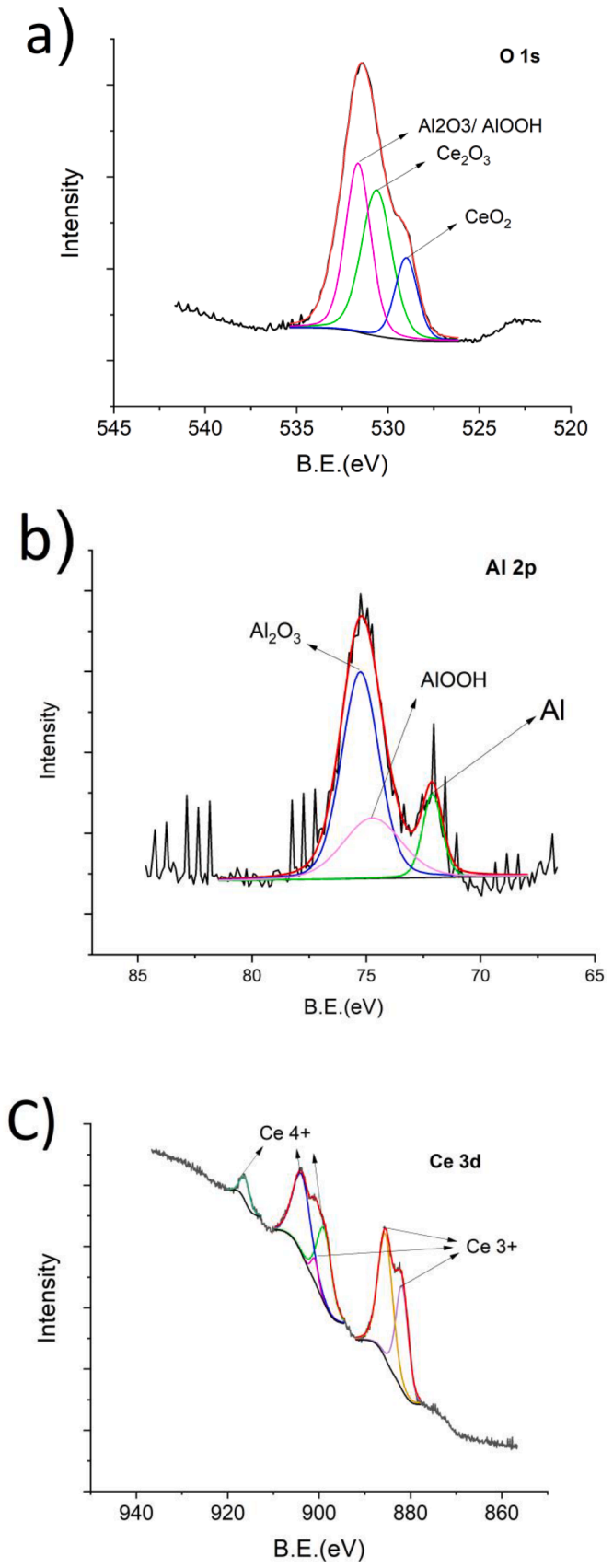

Fig. 6. XPS analysis of CeCC samples. High resolution spectra for a) O 1 s, b) Al 2p, and c) Ce 3d

Table 4
Mean values and standard deviations of the roughness and contact angle of the samples after different surface treatments.

Sample	Ra (μm)	Contact angle (°)
REF (AE+*D*)	0.451 ± 0.73	70.76 ± 6.05
SA	0.820 ± 0.83	12.54 ± 1.51
REF (P)	0.021 ± 0.002	51.46 ± 4.62
CeCC	0.041 ± 0.006	102.62 ± 0.51

value of about 71 °, while the reference alloy (P) shows a contact value of about 51°, which corresponds to a hydrophilic surface. Anodized samples, SA, show a highly hydrophilic behavior with lower contact angles around 14° Finally, the cerium conversion coated sample has a hydrophobic behavior with a contact angle of ~102°

The variations in wettability could be due to the changes in surface chemistry with different surface treatments, but it is also possible that topography plays a role. The topographical variations obtained after anodizing both at the macro and nanoscale scale could explain the decrease in hydrophobicity compared to the reference alloy, since the water droplet could be sucked into the pores.

3.3. *Bacterial adherence*

Adherence and survival are variables dependent on the type of bacteria and also on the properties of the material in which they are found, together with the environmental conditions [4]. It is important to note that artificial surfaces, including medical devices, have been shown to be a preferential site of adhesion for bacteria [43]. The first step in the adhesion process is the still reversible early stage of biofilm formation [44]. In this study we aimed to evaluate the adherence of *P. aeruginosa,* considered to be one of the most dangerous microorganisms associated with Healthcare associated Infections [45]. This microorganism is an environmental species that can be found in many sources, including medical ones. To our knowledge, only one study to date has evaluated the behaviour of *P. aeruginosa* on AA6063 nanostructured material, but with a different modification treatment [46].

Fig. 7 shows the results of the bacterial adherence study. The variables measured in the experiment were count (n), area (%), viability (%) and concentration of planktonic bacteria in the supernatant (CFU/ml). A lower adherence to the anodized and cerium coated surfaces was observed for P. aeruginosa compared to the AA6063 reference samples, as the count and area decreased significantly by 89.7 % (p <0,0001) and 94.7% (p <0,0001) respectively, in the case of the anodized samples. However, the cerium conversion coating showed no significant difference in any case. In addition, a significant increase in bacterial viability was observed for both surface treatments, SA and CeCC, although in the case of the CeCC there were cases where a decrease in bacterial viability was found. The results also showed a potential bactericidal effect of the SA samples compared to the reference samples due to a 65.4% reduction in the concentration of planktonic bacteria in the supernatant exposed to this material (p< 0,05). In presence of *P. aeruginosa*, the reference alloy released 16 (14,75–16,25) μg/mL, SA released 144,5 (107,5–152,6) μg/mL, while CeCC released 31,5 (20,5–52,6) μg/mL. From this aluminium released, *P. aeruginosa* uptook 59,8 (44.1–67,9)%, 65,1 (62,8–70,2)%, and 63,9 (56,9–65,6)% when it was exposed to the reference, SA, and CeCC alloys, respectively. These data are represented in Fig. 8.

The results show that the anodized surface has bacterial anti-adherent properties against *P. aeruginosa*, that outperform the cerium conversion coating. Literature pointed out that the nanostructured topography developed on the aluminium alloy 6063 by chemical etching shows a bactericidal behaviour, because the bacterial membrane is stretched to its maximum capacity until it is ruptured by the direct contact with the nanopillars grown during the chemical etching [46]. Therefore, the finding found in the present work could be related to the nanostructured surface topography formed on the aluminium alloy 6063

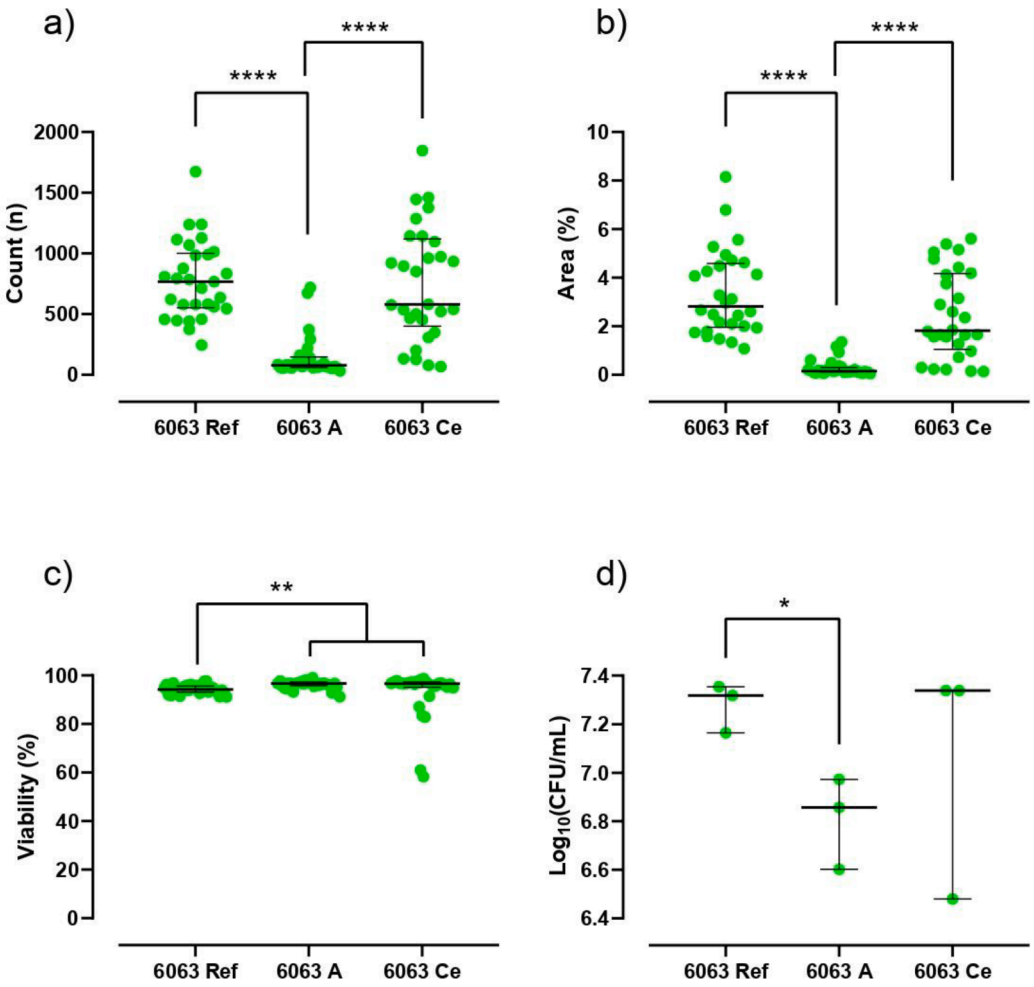

Fig. 7. Bacterial counts (a), area (b), adhered bacterial viability (c), and bacterial concentration in the supernatant (d) of P. aeruginosa (green) from the non-modified AA6063 (6063 Ref), anodized AA6063 (6063 A) and cerium conversion coating AA6063 (6063 Ce): p-value<0.05; **:p-value<0.01; ***:p-value<0.001; ****:p-value<0.0001.

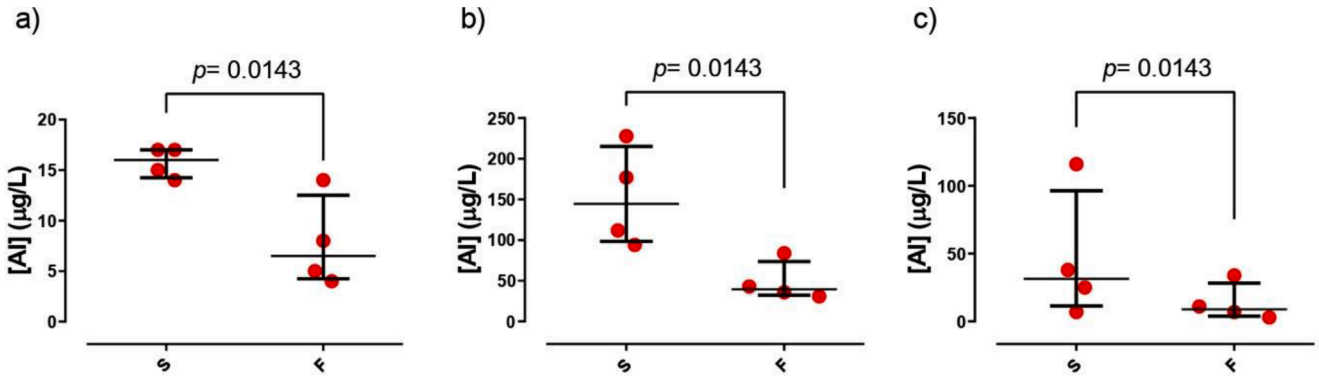

Fig. 8. Concentration of released and detected Al (III) in serum exposed to bacteria (S) and serum filtered not exposed to bacteria (F) from each of the surfaces: reference (a), anodized (b), and cerium conversion coating (c). The bar represents the interquartile range.

as a result of the anodizing process (nanoporous). This discrete change in the nanotopography and chemical composition of the metallic surface could affect the interaction between some filamentous appendages of the bacterial cell and the alloy, e.g. type IV pili, which have been shown to be essential for adhesion to abiotic and biotic surfaces [47].

On the other hand, hydrophobicity also plays an important role in the bacterial attachment to the surface. In general, hydrophobic surfaces seem to be more susceptible to the adhesion to bacteria in comparison to hydrophilic surfaces. In nature, *P. aeruginosa* bacteria from the same population can be hydrophilic or hydrophobic [48]. Moreover, this bacterium is able to sense and respond to a surface, probably via specific pathways to adapt its physiological response accordingly [49]. Under our experimental conditions, the number of adhering bacteria would mainly depend on the Lifshitz-van der Waals, Lewis acid-base and roughness properties of the materials, or in other words on their hydrophobic/hydrophilic properties [50].

Our study showed that planktonic *P. aeruginosa* bacteria exposed to the SA alloy decreased their viability (CFUs per ml), but the adherent bacteria were mainly viable. The planktonic bacteria from the supernatant of SA have lost their viability due to the toxicity of aluminium. It is well documented that the aluminium ion is toxic to microorganisms [51]. Although the mechanism of Al toxicity is not yet fully understood, it is known that Al ions can bind to the hydrophilic heads of cell membrane phospholipids and proteins by altering lipid-protein interactions and modifying transport activity; it can influence metabolism by binding to enzymes or enzyme substrates and destabilise and replace magnesium or calcium in biological systems and promote acidification of the medium [51]. *P. aeruginosa* produces two siderophores: pyochelin, which binds to Fe^{3+} in a 2:1 ratio, and pyoverdine, which binds to Fe^{+3} in a 1:1 ratio. These siderophores interact with specific outer membrane receptors [52], namely, the Fe(III)-pyochelin receptor (FptA) [53] and the Fe(III)-pyoverdine receptor (FpvA) [54]. These receptors facilitate the entry of aluminium(III)-siderophore into the periplasmic space [23, 55–59]. However, while aluminum- pyoverdine can be expelled from the periplasm to the extracellular space via an ATP-dependent efflux system resembling the PvdRT-OpmQ efflux system observed in *P. aeruginosa* PA01, there is no known similar efflux system for aluminum-pyochelin [23,55]. Consequently, aluminum-pyochelin might remain trapped in the periplasm, where aluminum exerts its bactericidal action, as demonstrated in the literature [23,60,61].

The viability of surface-adherent bacteria may be explained by the adaptability of this bacterial species to metallic surfaces, e.g. stainless steel, as it has been shown to be able to reduce the abundance of its porins to reduce the permeability of the outer membrane and other proteins associated with its cell wall homeostasis [49]. It is noteworthy that a similar reduction in porin content in the outer membrane of *P. aeruginosa* in response to copper-induced stress has already been described [62]. Our results are in contrast to previous studies that found a reduction in the viability of *S. aureus, S. epidermidis* and *Stenotrophomonas maltophilia* on an nanostructured anodized Ti-Al-V alloy able to release aluminium [23].

In the present case, the results suggest that both the nanostructured surface topography and the hydrophilicity exhibited for anodized samples, SA, are the responsible for the bacterial anti-adhesion and bactericidal properties.

4. Conclusions

The surface modification of aluminium alloy 6063 by the growth of anodic layers and by the deposition of cerium conversion coatings was investigated to prevent bacterial adhesion. Anodic layers with nanoporous morphology and thicknesses of 7 μm were grown. Cerium conversion coatings composed of a mixture of alumina/aluminium hydroxide and cerium oxides (Ce^{3+} and Ce^{4+}) and a globular structure were deposited.

An increased roughness of the reference samples was measured after anodizing, whereas no roughness differences were obtained after cerium conversion coatings deposition. The cerium conversion coatings showed a hydrophobic behavior, while anodized samples showed a higher wettability (lower contact angle values) compared to the bare alloy.

The results of the antimicrobial tests indicated that the cerium conversion coating did not show statistically significant antibacterial adhesion properties when compared to the reference alloy. Finally, the anodized sample shows enhanced antibacterial properties for *P. aeruginosa* ATCC27853 compared to the reference alloy and a potential bactericidal effect. This behaviour is due to the nanostructured surface topography and surface hydrophilicity resulting from the growth of the anodic layer. This could have potentially important implications for the prevention of the transmission of infections in hospital settings.

CRediT authorship contribution statement

M. Medel-Plaza: Data curation, Methodology, Writing – original draft, Writing – review & editing. **A. Conde:** Conceptualization, Formal analysis, Funding acquisition, Project administration, Writing – review & editing, Methodology. **J.J. de Damborenea:** Conceptualization, Funding acquisition, Project administration, Supervision, Writing – review & editing. **J.J. Aguilera-Correa:** Supervision, Writing – review & editing, Methodology. **J. Esteban:** Conceptualization, Methodology, Supervision, Writing – review & editing. **M.A. Arenas:** Conceptualization, Funding acquisition, Investigation, Supervision, Validation, Writing – original draft, Writing – review & editing.

Declaration of competing interest

The authors declare that they have no known competing financial interests or personal relationships that could have appeared to influence the work reported in this paper.

Data availability

Data will be made available on request.

Acknowledgements

This work was supported by Ministerio de Ciencia e Innovación (MICINN) PID2020-112878RB-100/AEI/10.13039/501100011033 - Development of Antimicrobial metallic surfaces-; the European Commission-Next Generation EU (Regulation EU2020/2024) through CSICs Global Health Platform and, PIE-CSIC 202060E194 and, CIBERINFEC-CIBER de Enfermedades Infecciosas (Centro de Investigación en Red de Enfermedades Infecciosas).

References

[1] J.S. Greatorex, P. Digard, M.D. Curran, R. Moynihan, H. Wensley, T. Wreghitt, H. Varsani, F. Garcia, J. Enstone, J.S. Nguyen-Van-Tam, Survival of influenza A (H1N1) on materials found in households: implications for infection control, PLoS. One 6 (2011) e27932, https://doi.org/10.1371/journal.pone.0027932.

[2] E. Ruiz-Hitzky, M. Darder, B. Wicklein, C. Ruiz-Garcia, R. Martín-Sampedro, G. del Real, P. Aranda, Nanotechnology responses to COVID-19, Adv. Healthcare Mater. 9 (2020) 2000979, https://doi.org/10.1002/adhm.202000979.

[3] B. Stephens, P. Azimi, M.S. Thoemmes, M. Heidarinejad, J.G. Allen, J.A. Gilbert, Microbial exchange via fomites and implications for human health, Curr. Pollut. Rep. 5 (4) (2019) 198–213, https://doi.org/10.1007/s40726-019-00123-6.

[4] A. Kramer, I. Schwebke, G. Kampf, How long do nosocomial pathogens persist on inanimate surfaces? A systematic review, BMC. Infect. Dis. 16 (6) (2006) 130, https://doi.org/10.1186/1471-2334-6-130.

[5] J.P. Barraza, M.A. Whiteley, Pseudomonas aeruginosa antimicrobial affects the biogeography but not fitness of staphylococcus aureus during coculture, mBio 12 (2) (2021) e00047, https://doi.org/10.1128/mBio.00047-21. Mar 30;-21.

[6] A. Hernández, G. Yagüe, E. García Vázquez, M. Simón, L. Moreno Parrado, M. Canteras J. Gómez, Nosocomial infections caused by multiresistant pseudomonas aeruginosa (carbapenems included): predictive and prognostic factors. A prospective study (2016-2017), Rev. Esp. Quimioter. 31 (2) (2018) 123–130.

[7] D. Altenpohl, Aluminum: technology, applications and environment. A profile of a modern metal. Sixth Edition, 1998. Technical Editor. J. Gilbert kaufman TMS (The Minerals, Metals and Materials Society).

[8] J.J. Aguilera-Correa, J. Esteban, D. Romera-García, Mechanisms of biofilm formation in clinically used biomaterials. In Mitra A ed. Microbial Biofilms: Current Research and Practical Implications, Caister Academic Press, United Kingdom, 2020, pp. 135–194, https://doi.org/10.21775/9781912530328.04.

[9] M.O. Aydogdu, E. Altun, E. Chung, G. Ren, S. Homer-Vanniasinkam, B. Chen, M. Edirisinghe, 2021 Surface interactions and viability of coronaviruses, J. R. Soc. Interface. 18 (2020) 0798, https://doi.org/10.1098/rsif.2020.0798.

[10] B. Balasubramaniam, S. Ranjan, M. Saraf, P. Kar, S.P. Singh, V.K. Thakur, A. Singh, R.K. Gupta, Antibacterial and antiviral functional materials: chemistry and biological activity toward tackling COVID-19-like Pandemics, ACS. Pharmacol. Transl. Sci. 4 (1) (2021) 8–54, https://doi.org/10.1021/acsptsci.0c00174.

[11] A. Nouri, A.R. Shirvan, Y. Li, C. Wen, Surface modification of additively manufactured metallic biomaterials with active antipathogenic properties, Smart Mate. Manufact. 1 (2023) 100001, https://doi.org/10.1016/j.smmf.2022.100001.

[12] A. Frei, A.D. Verderosa, A.G. Elliott, J. Zuegg, M.A.T. Blaskovich, Metals to combat antimicrobial resistance, Nat. Rev. Chem. 7 (3) (2023) 202–224, https://doi.org/10.1038/s41570-023-00463-4.
[13] J. Jann, O. Drevelle, X.G. Chen, M. Auclair-Gilbert, G. Soucy, N. Faucheux, L. C. Fortier, Rapid antibacterial activity of anodized aluminum-based materials impregnated with quaternary ammonium compounds for high-touch surfaces to limit transmission of pathogenic bacteria, RSC. Adv. 26 (60) (2021) 38172–38188, https://doi.org/10.1039/d1ra07159a, 11.
[14] E. Barker, J. Shepherd, I.O. Asencio, The use of cerium compounds as antimicrobials for biomedical applications, Molecules 21 (9) (2022) 2678, https://doi.org/10.3390/molecules27092678, 27.
[15] I. Celardo, J.Z. Pedersen, E. Traversa, L. Ghibelli, Pharmacological potential of cerium oxide nanoparticles, Nanoscale 3 (2011) 1411–1420, https://doi.org/10.1039/C0NR00875C.
[16] D.A. Pelletier, A.K. Suresh, G.A. Holton, C.K. McKeown, W. Wang, B. Gu, N. P. Mortensen, D.P. Allison, D.C. Joy, M.R. Allison, S.D. Brown, T.J. Phelps, M. J. Doktycz, Effects of engineered cerium oxide nanoparticles on bacterial growth and viability, Appl. Environ. Microbiol. 76 (24) (2010) 7981–7989, https://doi.org/10.1128/AEM.00650-10.
[17] A. Thill, O. Zeyons, O. Spalla, F. Chauvat, J. Rose, M. Auffan, A.M. Flank, Cytotoxicity of CeO2 nanoparticles for escherichia coli. Physico-chemical insight of the cytotoxicity mechanism, Environ. Sci. Technol. 40 (19) (2006) 6151–6156, https://doi.org/10.1021/es060999b.
[18] Y.N. Slavin, U.O.Häfeli J.Asnis, H. Bach, Metal nanoparticles: understanding the mechanisms behind antibacterial activity, J Nanobiotechnol 15 (1) (2017) 65–84, https://doi.org/10.1186/s12951-017-0308-z.
[19] D. Predoi, S.L. Iconaru, M.V. Predoi, A. Groza, S. Gaiaschi, K. Rokosz, S. Raaen, C. C. Negrila, Prodan A-M, A. Costescu, M.L. Badea, P. Chapon, Development of cerium-doped hydroxyapatite coatings with antimicrobial properties for biomedical applications, Coatings 10 (6) (2020) 516, https://doi.org/10.3390/coatings10060516.
[20] C. Perez-Jorge, M.A. Arenas, A. Conde, J.M. Hernández-Lopez, J.J. De Damborenea, S. Fisher, A.M.A. Hunt, J. Esteban, G. James, Bacterial and fungal biofilm formation on anodized titanium alloys with fluorine, J Mater Sci: Mater Med 28 (2017) 8, https://doi.org/10.1007/s10856-016-5811-5.
[21] D. Asker, T.S. Awad, D. Raju, H. Sanchez, I. Lacdao, S. Gilbert, P. Sivarajah, D. R. Andes, D.C. Sheppard, P.L. Howell, B.D. Hatton, Preventing Pseudomonas aeruginosa biofilms on indwelling catheters by surface-bound enzymes, ACS. Appl. Bio Mater. 4 (2021) 8248–8258, https://doi.org/10.1021/acsabm.1c00794.
[22] W. Zhang, J. Sun, W. Ding, J. Lin, R. Tian, L. Lu, X. Liu, X. Shen, P.Y. Qian, Extracellular matrix-associated proteins form an integral and dynamic system during Pseudomonas aeruginosa biofilm development, Front. Cell Infect. Microbiol. 5 (2015). https://www.frontiersin.org/articles/10.3389/fcimb.2015.00040. accessed December 5, 2022.
[23] J.J. Aguilera-Correa, A. Mediero, F.M. Conesa-Buendía, A. Conde, M.A. Arenas, J. J. de Damborenea, J. Esteban, Microbiological and cellular evaluation of a fluorine-phosphorus-doped titanium alloy, a novel antibacterial and osteostimulatory biomaterial with potential applications in orthopedic surgery, Appl. Environ. Microbiol. 85 (2019) e02271, https://doi.org/10.1128/AEM.02271-18. -18.
[24] M.A. Arenas, C. Pérez-Jorge, A. Conde, E. Matykina, J.M. Hernández-López, R. Pérez-Tanoira, J.J. de Damborenea, E. Gómez-Barrena, J. Esteban, Doped TiO2 anodic layers of enhanced antibacterial properties, Biointerfaces 105 (2013) 106–112, https://doi.org/10.1016/j.colsurfb.2012.12.051.
[25] C. Pérez-Jorge, A. Conde, M.A. Arenas, R. Pérez-Tanoira, E. Matykina, J.J. de Damborenea, E. Gómez-Barrena, J. Esteban, vitro assessment of Staphylococcus epidermidis and Staphylococcus aureus adhesion on TiO2 nanotubes on Ti–6Al–4V alloy, J. Biomed. Mater. Res. A 100A (2012) 1696–1705, https://doi.org/10.1002/jbm.a.34118.
[26] T.J. Kinnari, J. Esteban, E. Gomez-Barrena, N. Zamora, R. Fernandez-Roblas, A. Nieto, J.C. Doadrio, A. López-Noriega, E. Ruiz-Hernández, D. Arcos, M. Vallet-Regí, Bacterial adherence to SiO2-based multifunctional bioceramics, J. Biomed. Mater. Res. Part A 89A (2009) 215–223, https://doi.org/10.1002/jbm.a.31943.
[27] L. Boulos, M. Prévost, B. Barbeau, J. Coallier, R. Desjardins, LIVE/DEAD® baclightTM: application of a new rapid staining method for direct enumeration of viable and total bacteria in drinking water, J. Microbiol. Meth. 37 (1999) 77–86, https://doi.org/10.1016/S0167-7012(99)00048-2.
[28] B. Herigstad, M. Hamilton, J. Heersink, How to optimize the drop plate method for enumerating bacteria, J. Microbiol. Meth. 44 (2001) 121–129, https://doi.org/10.1016/S0167-7012(00)00241-4.
[29] L. Aydi, M. Khlifa, C. Bradaia, S. Spigarellib, M. Cabibbob, M. El Mehtedib, Mechanical properties and microstructure of primary and secondary aa6063 aluminum alloy after extrusion and T5 heat treatment, Proceedings 2 (10) (2015) 4890–4897, https://doi.org/10.1016/j.matpr.2015.10.044.
[30] G. Mrówka-Nowotnik, J. Sieniawski, M. Wierzbińska, Analysis of intermetallic particles in AlSi1MgMn aluminium alloy, J. Achiev. Mater. Manufact. Eng. 20 (1–2) (2007) 155–158.
[31] P.G. Sheasby, R. Pinner, The surface treatment and finishing of aluminium alloys, 1, ASM International. Finishing Publications Ltd, 2001.
[32] M. Schneider, W. Fürbeth, Anodizing—The pore makes the difference, Mater. Corros. 73 (2022) 1752–1765, https://doi.org/10.1002/maco.202213324.
[33] M. Saenz de Miera, M. Curioni, P. Skeldon, G.E. Thompson, The behaviour of second phase particles during anodizing of aluminium alloys, Corros. Sci. 52 (2010) 2489–2497, https://doi.org/10.1016/j.corsci.2010.03.029.
[34] G.E. Thompson, P. Skeldon, X. Zhou, K. Shimizu, H. Habazaki, C.J.E. Smith, Improving the performance of aerospace alloys, Aircr. Eng. Aerosp. Tec. 75 (2003) 372–379, https://doi.org/10.1108/00022660310484301.
[35] X. Zhou, G.E. Thompson, P. Skeldon, G.C. Wood, K. Shimizu, H. Habazaki, Film formation and detachment during anodizing of Al–Mg alloys, Corr. Sci. 41 (1999) 1599–1613, https://doi.org/10.1016/S0010-938X(99)00007-4.
[36] Y. Liu, P. Skeldon, G.E. Thompson, H. Habazaki, K. Shimizu, Anodic film growth on an Al–21at.%Mg alloy, Corr. Sci. 44 (2002) 1133–1142, https://doi.org/10.1016/S0010-938X(01)00115-9.
[37] Y. Liu, M.A. Arenas, P. Skeldon, G.E. Thompson, P. Bailey, T.C.Q. Noakes, H. Habazaki, K. Shimizu, Anodic behaviour of a model second phase: al–20at.% Mg–20at.%Cu, Corr. Sci. 48 (2006) 1225–1248, https://doi.org/10.1016/j.corsci.2005.05.007.
[38] H.D. Johansen, C.M.A. Brett, A.J. Motheo, Corrosion protection of aluminium alloy by cerium conversion and conducting polymer duplex coatings, Corr. Sci. 63 (2012) 342–350, https://doi.org/10.1016/j.corsci.2012.06.020.
[39] M. Hoang, A.E. Hughes, T.W. Turney, An XPS study of Ru-promotion for Co/CeO2 fischer-tropsch catalyst, Appl. Surf. Sci. 72 (1993) 55–65, https://doi.org/10.1016/0169-4332(93)90043-B.
[40] S. Chang, M. Li, Q. Hua, L. Zhang, Y. Ma, B. Ye, W. Huang, Shape-dependent interplay between oxygen vacancies and Ag–CeO2 interaction in Ag/CeO2 catalysts and their influence on the catalytic activity, J. Catal. 293 (2012) 195–204, https://doi.org/10.1016/j.jcat.2012.06.025.
[41] M. Liu, X. Wu, S. Liu, Y. Gao, Z. Chen, Y. Ma, R. Ran, D. Weng, Study of Ag/CeO2 catalysts for naphthalene oxidation: balancing the oxygen availability and oxygen regeneration capacity, Appl. Catal. B 219 (2017) 231–240, https://doi.org/10.1016/j.apcatb.2017.07.058.
[42] Ch. Girginov, S. Kozhukharov, M. Milanes, M. Machkova, Impact of the anodizing duration on the surface morphology and performance of A2024-T3 in a model corrosive medium, Mater. Chem. Phys. 198 (2017) 137–144, https://doi.org/10.1016/j.matchemphys.2017.05.049.
[43] C. Wagner, S. Aytac, G.M. Hänsch, Biofilm growth on implants: bacteria prefer plasma coats, Int. J. Artif. Organs 34 (2011) 811–817, https://doi.org/10.5301/ijao.5000061.
[44] J.W. Costerton, P.S. Stewart, E.P. Greenberg, Bacterial biofilms: a common cause of persistent infections, Science (1979) 284 (1999) 1318–1322, https://doi.org/10.1126/science.284.5418.1318.
[45] M.T.T. Thi, D. Wibowo, B.H.A. Rehm, Pseudomonas aeruginosa Biofilms, Int. J. Mol. Sci. 21 (2020) 8671, https://doi.org/10.3390/ijms21228671.
[46] J. Hasan, Y. Xu, T. Yarlagadda, M. Schuetz, K. Spann, P.K. Yarlagadda, Antiviral and antibacterial nanostructured surfaces with excellent mechanical properties for hospital applications, ACS. Biomater. Sci. Eng. 6 (2020) 3608–3618, https://doi.org/10.1021/acsbiomaterials.0c00348.
[47] A. Beaussart, A.E. Baker, S.L. Kuchma, S. El-Kirat-Chatel, G.A. O'Toole, Y. F. Dufrêne, Nanoscale adhesion forces of pseudomonas aeruginosa Type IV Pili, ACS. Nano 8 (2014) 10723–10733, https://doi.org/10.1021/nn5044383.
[48] C.o. Obuekwe, Z.k. Al-Jadi, E.s. Al-Saleh, Comparative hydrocarbon utilization by hydrophobic and hydrophilic variants of Pseudomonas aeruginosa, J. Appl. Microbiol. 105 (2008) 1876–1887, https://doi.org/10.1111/j.1365-2672.2008.03887.x.
[49] M. Guilbaud, J. Bruzaud, E. Bouffartigues, N. Orange, A. Guillot, A. Aubert-Frambourg, V. Monnet, J.M. Herry, S. Chevalier, M.N. Bellon-Fontaine, Proteomic response of pseudomonas aeruginosa PAO1 adhering to solid surfaces, Front. Microbiol. 8 (2017) 1465, https://doi.org/10.3389/fmicb.2017.01465.
[50] J. Bruzaud, J. Tarrade, A. Coudreuse, A. Canette, J.M. Herry, E. Taffin de Givenchy, T. Darmanin, F. Guittard, M. Guilbaud, M.N. Bellon-Fontaine, Flagella but not type IV pili are involved in the initial adhesion of Pseudomonas aeruginosa PAO1 to hydrophobic or superhydrophobic surfaces, Colloids. Surf. B Biointerfaces 131 (2015) 59–66, https://doi.org/10.1016/j.colsurfb.2015.04.036.
[51] R.G. Piña, C. Cervantes, Microbial interactions with aluminium, Biometals 9 (1996) 311–316, https://doi.org/10.1007/BF00817932.
[52] C. Baysse, J.M. Meyer, P. Plesiat, V. Geoffroy, Y. Michel-Briand, P. Cornelis, Uptake of pyocin S3 occurs through the outer membrane ferripyoverdine type II receptor of pseudomonas aeruginosa, J. Bacteriol. 181 (1999) 3849–3851.
[53] R.G. Ankenbauer, H.N. Quan, FptA, the Fe(III)-pyochelin receptor of Pseudomonas aeruginosa: a phenolate siderophore receptor homologous to hydroxamate siderophore receptors, J. Bacteriol. 176 (1994) 307–319, https://doi.org/10.1128/jb.176.2.307-319.1994.
[54] J.M. Meyer, A. Stintzi, K. Poole, The ferripyoverdine receptor FpvA of Pseudomonas aeruginosa PAO1 recognizes the ferripyoverdines of P aeruginosa PAO1 and P fluorescens ATCC 13525, FEMS Microbiol. Lett. 170 (1999) 145–150, https://doi.org/10.1111/j.1574-6968.1999.tb13367.x.
[55] I.J. Schalk, M. Hannauer, A. Braud, New roles for bacterial siderophores in metal transport and tolerance, Environ. Microbiol. 13 (2011) 2844–2854, https://doi.org/10.1111/j.1462-2920.2011.02556.x.
[56] I.J. Schalk, Metal trafficking via siderophores in Gram-negative bacteria: specificities and characteristics of the pyoverdine pathway, J. Inorg. Biochem. 102 (2008) 1159–1169, https://doi.org/10.1016/j.jinorgbio.2007.11.017.
[57] A. Braud, F. Hoegy, K. Jezequel, T. Lebeau, I.J. Schalk, New insights into the metal specificity of the Pseudomonas aeruginosa pyoverdine–iron uptake pathway, Environ. Microbiol. 11 (2009) 1079–1091, https://doi.org/10.1111/j.1462-2920.2008.01838.x.
[58] A. Braud, M. Hannauer, G.L.A. Mislin, I.J. Schalk, The pseudomonas aeruginosa pyochelin-iron uptake pathway and its metal specificity, J. Bacteriol. 191 (2009) 3517–3525, https://doi.org/10.1128/jb.00010-09.

[59] J. Greenwald, G. Zeder-Lutz, A. Hagege, H. Celia, F. Pattus, The metal dependence of pyoverdine interactions with its outer membrane receptor FpvA, J. Bacteriol. 190 (2008) 6548–6558, https://doi.org/10.1128/jb.00784-08.
[60] J.A. Lemire, J.J. Harrison, R.J. Turner, Antimicrobial activity of metals: mechanisms, molecular targets and applications, Nat. Rev. Microbiol. 11 (2013) 371–384, https://doi.org/10.1038/nrmicro3028.
[61] J.J. Aguilera-Correa, Á. Auñón, M. Boiza-Sánchez, I. Mahillo-Fernández, A. Mediero, D. Eguibar-Blázquez, A. Conde, M.Á. Arenas, J.J. de-Damborenea, J. Cordero-Ampuero, J. Esteban, Urine aluminum concentration as a possible implant biomarker of pseudomonas aeruginosa infection using a fluorine- and phosphorus-doped Ti-6Al-4V alloy with osseointegration capacity, ACS. Omega 4 (2019) 11815–11823, https://doi.org/10.1021/acsomega.9b00898.
[62] G.M. Teitzel, A. Geddie, S.K. De Long, M.J. Kirisits, M. Whiteley, M.R. Parsek, Survival and growth in the presence of elevated copper: transcriptional profiling of copper-stressed pseudomonas aeruginosa, J. Bacteriol. 188 (2006) 7242–7256, https://doi.org/10.1128/JB.00837-06.